Special Section Brief Papers

Feedback-Linearized Inverse Feedforward for Creep, Hysteresis, and Vibration Compensation in AFM Piezoactuators

Kam K. Leang, *Member, IEEE*, and Santosh Devasia, *Senior Member, IEEE*

***Abstract*—In this brief, we study the design of a feedback and feedforward controller to compensate for creep, hysteresis, and vibration effects in an experimental piezoactuator system. First, we linearize the nonlinear dynamics of the piezoactuator by accounting for the hysteresis (as well as creep) using high-gain feedback control. Next, we model the linear vibrational dynamics and then invert the model to find a feedforward input to account vibration—this process is significantly easier than considering the complete nonlinear dynamics (which combines hysteresis and vibration effects). Afterwards, the feedforward input is augmented to the feedback-linearized system to achieve high-precision high-speed positioning. We apply the method to a piezoscanner used in an experimental atomic force microscope to demonstrate the method's effectiveness and we show significant reduction of both the maximum and root-mean-square tracking error. For example, high-gain feedback control compensates for hysteresis and creep effects, and in our case, it reduces the maximum error (compared to the uncompensated case) by over 90%. Then, at relatively high scan rates, the performance of the feedback controlled system can be improved by over 75% (i.e., reduction of maximum error) when the inversion-based feedforward input is integrated with the high-gain feedback controlled system.**

***Index Terms*—Creep, feedback control, high-precision positioning, hysteresis, inversion-based feedforward control, piezoactuator, vibration.**

I. Introduction

In this brief, we address positioning errors caused by the adverse effects of creep, hysteresis, and vibrational dynamics in an experimental piezo-positioning system. When piezoactuators are used, for example, in scanning probe microscopy (SPM) applications, high-precision high-speed positioning of the probe tip relative to a sample surface is critical for observing and manipulating objects at the nanoscale. For instance, nanoindents created with the SPM probe tip are exploited to initiate the growth of quantum dots (QDs)—QDs nucleate at the "indent" sites [1]. However, the quality of the QDs are greatly affected by the size and spacing of the indents—even 2–4 nm variation in size and spacing of QDs can drastically alter their energy density and electronic-band structure [2]. Being a serial technique, the throughput of the SPM-based indentation process is directly proportional to the speed at which the SPM probe tip is positioned. Therefore, high-precision high-speed control of the piezo positioner in SPMs is needed, for example, to enable QD cellular automata technologies for creating novel digital-logic devices [3]. But, unfortunately, the effects of creep, hysteresis, and the vibration in piezos present a major challenge. Although previous work showed that model-based inversion can be used to find feedforward inputs to correct for these effects [4], both modeling the complete nonlinear dynamics and inverting it to find an input can be difficult due to the inherent model complexity and uncertainty. In contrast, the main contribution of this brief is presenting an approach that first linearizes the nonlinear dynamics by using relatively high-gain feedback to account for the hysteresis (as well as creep). Then, the linear vibrational dynamics is modeled and inverted to find a feedforward input to account for vibration. This decoupled approach is significantly easier than modeling the complete nonlinear dynamics and finding a feedforward input using the nonlinear model.

The effects of creep, hysteresis, and vibration limit the performance of piezo-positioning systems. For example, creep (or drift) effect leads to significant error when positioning over extended periods of time (e.g., during slow-speed scanning operations) [5]. Hysteresis, a nonlinear behavior between the applied electric field and the mechanical displacement of the piezoactuator [6], leads to loss in precision when operating over relatively long-range displacements [7]. When the output is scanned at high frequencies relative to the first resonance vibrational frequency of the piezo-positioner, movement-induced oscillation leads to significant positioning error [8]. Typically, scan rates (or scan frequencies) are restricted to less than 1/10th to 1/100th of the first resonance frequency, thus limiting the operating bandwidth of piezo-based systems.

Numerous studies have been done to develop techniques to compensate for these three adverse effects in piezo positioners. In general, they can be categorized as either feedback or model-based feedforward control. For instance, feedback-based control has demonstrated substantial improvement in performance, e.g., see the works [7], [9]–[11]. The advantages of feedback-based methods include: 1) the ability to handle modeling errors and 2) the robustness to parameter variation due to aging effects and environmental changes,

Manuscript received May 8, 2006; revised October 13, 2006. Manuscript received in final form December 26, 2006. Recommended by Guest Editor E. Eleftheriou. This work was supported by the National Science Foundation under Grant CMS 0301787.

K. K. Leang is with the Department of Mechanical Engineering, Virginia Commonwealth University, Richmond, VA 23284-3015 USA (e-mail: kkleang@vcu.edu).

S. Devasia is with the Mechanical Engineering Department, University of Washington, Seattle, WA 98195-2600 USA (e-mail: devasia@u.washington.edu).

Color versions of one or more of the figures in this paper are available online at http://ieeexplore.ieee.org.

Digital Object Identifier 10.1109/TCST.2007.902956

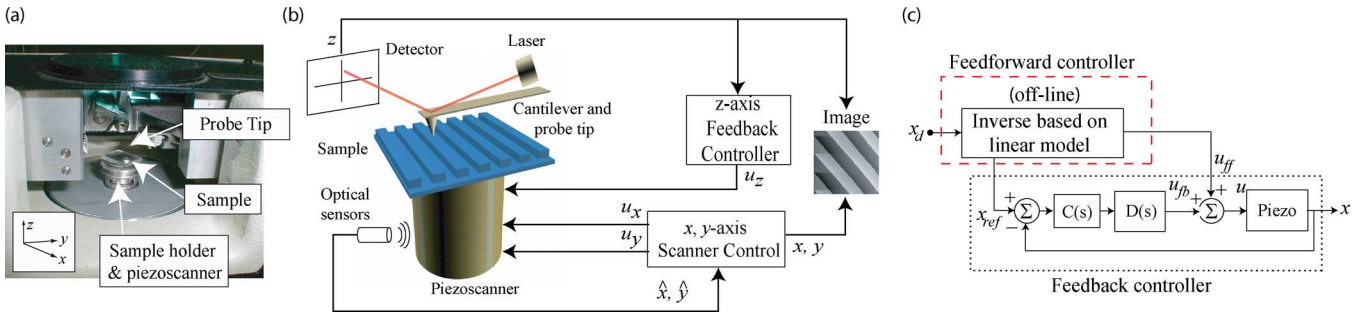

Fig. 1. (a), (b) The AFM system. A piezoscanner is used to place a sample relative to the cantilever and probe tip. The schematic shows the connections for the input and output signals. (c) Block diagram of the x-axis control system (y-axis is similar), where $u_{\rm ff}$ and $u_{\rm fb}$ are the feedforward and feedback inputs, respectively, u is the input to the system, $C(s)$ is the feedback controller, $D(s)$ is the notch filter for improving gain margin, $x_{\rm ref}$ is the reference trajectory to the feedback system, and x is the actual system output along the x-axis.

such as temperature [12]. However, feedback control provides limited vibrational-dynamics compensation [7]. On the other hand, feedforward-based methods account for all three effects. Various models (such as the Preisach hysteresis model) have been exploited to find feedforward input to minimize creep and hysteresis effects, e.g., see [13]–[16]. By carefully modeling the coupled creep, hysteresis, and vibration behaviors, an inversion-based feedforward approach was applied to find an input to improve positioning performance [4]. However, the major disadvantages are the coupled creep, hysteresis, and vibration effects, which are challenging to accurately model and invert. Furthermore, model-based approaches, especially those involving hysteresis models, lack robustness and they can be computationally cumbersome to implement.

The main contribution of this brief is presenting a control approach that uses: 1) relatively high-gain feedback to linearize the nonlinear dynamics (hysteresis and creep) and 2) feedforward input computed from the linear vibrational dynamics model to account for vibration. We note that such feedback/feedforward integration does not limit the choice of the feedback controller, that is, the model-based feedforward technique can be used with any of the existing or emerging feedback approaches [17] (the design of the two controllers is decoupled). Moreover, the integrated approach provides robustness to parameter variation and simplifies the computation of the feedforward input because modeling of the creep and hysteresis behaviors is not required. A second contribution of this brief is we address the relatively low gain margin of piezos due to low structural damping (i.e., sharp resonant peak which results in high quality factor Q_f) and additional piezo dynamics. Therefore, we improve the stability margin of the system and thereby enable high-gain feedback by modifying the sharp resonant peak of the system with a notch filter [9]—experimental results are presented to show that this approach can lead to a substantial increase in the measured gain margin (the gain margin was increased from -17.05 to 30.86 dB for our experimental system). To demonstrate the performance enhancement of the feedback/feedforward approach, we implement the approach and show experimental results from an AFM system where the piezoactuator is positioned over extended periods of time (through creep compensation), long ranges (through hysteresis compensation), and at high scan rates (through vibration compensation).

This brief is organized as follows. In Section II, we describe the AFM system and the modeling, followed by the design of a high-gain feedback controller in Section III. In Section IV, we discuss the feedforward approach and show experimental results. Finally, we present concluding remarks in Section V.

II. Modeling the Linear Vibrational Dynamics of the Experimental AFM Piezoscanner

In this section, we describe the experimental AFM system and the modeling of the linear vibrational dynamics of the piezoactuator (piezoscanner). (The linear model will be used later in Section IV to account for vibration effect.) The experimental AFM system studied in this brief utilizes a piezoscanner to position a probe tip relative to a sample surface as shown in Fig. 1(a) and (b). More specifically, the actuator is a sectored lead-zirconate-titanate (PZT) piezoelectric-tube actuator [18]. The linear vibrational dynamics model of the piezoscanner was obtained using a black-box identification technique, i.e., the model was found by curve fitting the system's measured frequency response. (For brevity, we describe the x-axis model—the model in the y-axis is similar.) The frequency response was measured using a commercially available dynamic signal analyzer (DSA, Stanford Research Systems Model SR785). A sinusoidal input voltage u generated by the DSA was applied to the piezoscanner. The resulting lateral displacement of the scanner (in the x-direction) was measured by an optical sensor (which has a static gain of 20 μm/V) and fed back to the DSA to construct the frequency response curve shown in Fig. 2(a) (solid line). The frequency response was measured over a displacement range of ± 2.00 μm, which is less than 5% of the maximum output range: a range where hysteresis is negligible. In addition, the frequency response was measured over a relatively high-frequency range (1 Hz to 2 kHz) to minimize creep effect.

A linear vibrational dynamics model—represented as a transfer function in the Laplace domain relating the input voltage u to the sensor output $\hat{x}$ of the piezoscanner was curve-fitted using MATLAB software to the measured frequency response. The model was found to be

$$\hat{G}(s) = \frac{\hat{x}(s)}{u(s)} = k_0 \frac{\prod_{m=1}^{2}(s - 2\pi z_m)}{\prod_{n=1}^{6}(s - 2\pi p_n)} \left(\frac{V}{V}\right) \qquad (1)$$

where $k_0 = 7.20 \times 10^{13}$ is the nominal system (or model) gain factor (i.e., measured over the ± 2.00- μm range). The zeros (z_m,

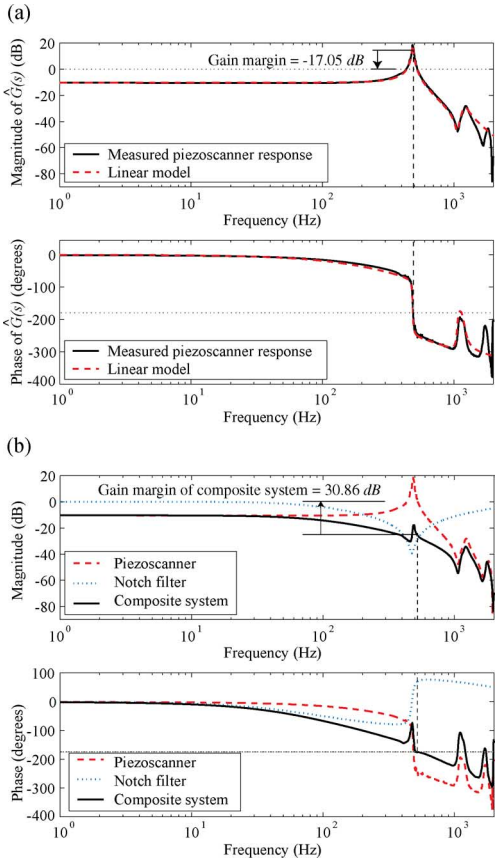

Fig. 2. (a) Frequency response of the experimental piezoscanner measured over small displacements (± 2 μm): measured (solid line) and linear model (dashed line). (b) Measured frequency response of the piezoscanner (dashed line), the notch filter (dotted line), and the notch filter cascaded with the piezoscanner (solid line). The measured gain margin of the original system is $-$ 17.05 dB, whereas the gain margin of the composite system is 30.86 dB.

for $m = 1, 2$) are $-25 \pm j1059$ (units hertz); and the poles (p_n, for $n = 1, \ldots, 6$) are -411, $-5 \pm j486$, $-70 \pm j1200$, -1200 (units hertz). The units of the transfer function $\hat{G}(s)$ is expressed in actual displacement units (micrometers/Volts) by multiplying $\hat{G}(s)$ with the static sensor gain 20 μm/V, i.e., $G(s) = 20\hat{G}(s)$ (μm/V). The linear single–input single–output (SISO) model [dashed line in Fig. 2(a)] is a good fit of the measured system response up to approximately 1.5 kHz [17]. We note that the linear model is only valid over small displacement ranges, and as the range increases, the effect of hysteresis can cause significant model uncertainty, for example, as shown in Section III-C, where hysteresis increases the system's gain factor k_0.

Remark: The sharp resonant peak at 486 Hz limits scanning to very low frequencies: typically 10 to 100 times lower than the first resonance frequency during high-precision applications. Therefore, open-loop scanning is limited to less than 5 Hz to avoid significant vibration effect.

III. High-Gain Feedback Linearization of Piezo-Dynamics

A. Improving the Gain Margin

Positioning errors in piezoactuators can be reduced with the use of feedback control; however, a problem with using feedback control is the issue with low-gain margin inherent in these systems. In particular, the experimental piezoscanner frequency response reveals the effect of low structural damping (i.e., sharp resonant peak or high-quality factor Q_f) along with additional dynamics (poles) which together pull the system's phase response below the -180° mark giving rise to low gain margin. For example, the experimental piezoscanner has a measured gain margin of -17.05 dB [see Fig. 2(b)]. Therefore, the proportional feedback gain is restricted to be less than 0.14 for stability of the closed-loop system. Such low-gain feedback controllers do not lead to significant improvement in the tracking response when compared to the open-loop system.

To enable the use of high-gain feedback control, the gain margin was increased by modifying, in particular, the sharp resonant peak of the open-loop system with a notch filter [as shown in Fig. 1(c)] [9]. The notch filter was chosen as

$$D(s) = k_D \frac{(s - 2\pi z_1)(s - 2\pi z_2)}{(s - 2\pi p_1)(s - 2\pi p_2)} \left(\frac{V}{V}\right) \tag{2}$$

where $k_D = 2.22$, $z_1 = -5 + j475$ Hz, $z_2 = -5 - j475$ Hz, $p_1 = -100$ Hz, and $p_2 = -5000$ Hz. In the design of the notch filter $D(s)$, the zeros were chosen to suppress the effect of the dominant resonant peak of the piezoactuator (at 486 Hz). The modification compensated for the significant decrease in phase (180°) caused by the resonant poles. The zeros of the notch filter $D(s)$ were placed at 475 Hz to achieve high gain margin for the composite system despite small changes in the location of the resonance frequency of the open-loop system. To ensure that $D(s)$ was proper, a pair of poles were added to the notch filter at 100 and 5000 Hz, and the poles helped to attenuate high-frequency noise. The notch filter was realized using analog op-amp circuits (e.g., [19, pp. 394–399]) and its measured frequency response is shown by the dotted line in Fig. 2(b), together with the superimposed frequency response of the original system (dashed line) for comparing the old and new gain margins. The frequency response of the composite system [solid line in Fig. 2(b)] shows significant increase in the gain margin from -17.05 to 30.86 dB.

B. High-Gain Feedback Controller Design

Hysteresis (and creep) can be minimized using high-gain feedback control. For example, with the gain margin significantly improved using the filter $D(s)$, a *proportional-plus-derivative* (PD) high-gain feedback controller of the form

$$C(s) = K_p + K_d \frac{\sigma^2 s}{(s + \sigma)^2} \left(\frac{V}{V}\right) \tag{3}$$

was used to linearize the response of the piezoscanner in the AFM. The objective was to show that large feedback gain (e.g., proportional gain) can be used to minimize hysteresis and creep effects after the notch filter was added. Although integral control has been applied for hysteresis and creep compensation, our objective was to show that by improving the gain margin, high proportional gain can be used to account for creep and hysteresis effect. We note that with the improved stability margin, an integral term can also be added to further improve performance of the feedback-controlled system.

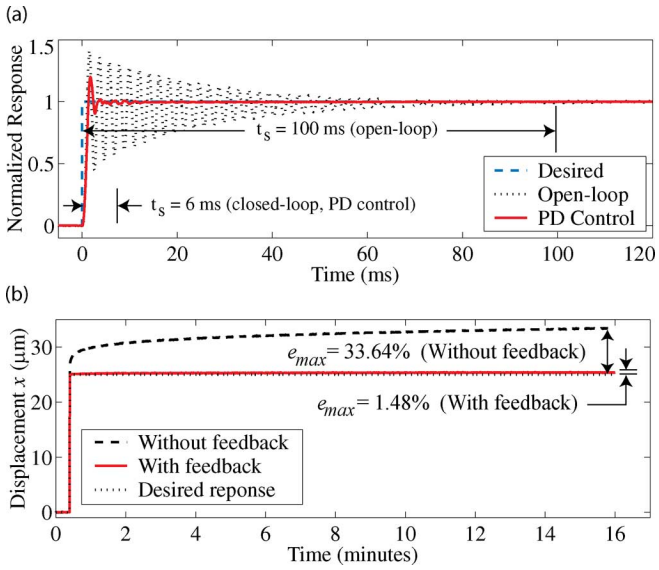

Fig. 3. (a) Step response comparing 2% settling time between open-loop (without notch filter $D(s)$) and closed-loop performance. The desired displacement is 25 μm. (b) Experimental results: creep compensation using high-gain feedback control. Dashed line is without compensation, solid line is with compensation, and dotted line is the desired response.

The proposed controller [see Fig. 1(c)] was implemented with analog op-amp circuits. The derivative gain in (3) helps improve the transient response, that is to help minimize oscillations. The two-poles in the derivative term (at 5000 Hz, i.e., $\sigma = 3.14 \times 10^4$ rad/s) attenuates high frequency noise that would otherwise amplified by differentiating the error signal. The feedback gains (K_p and K_d) were tuned experimentally (e.g., see [20, Sec. 4.5]); the controller gains were chosen to be $K_p = 20$ and $K_d = 6.56 \times 10^{-3}$. We note that without the filter $D(s)$, the proportional controller gain K_p was limited to 0.14 to ensure stability of the closed-loop system. However, the notch filter $D(s)$ enables the use of much larger feedback gain. Using $K_p = 20$ and $K_d = 6.56 \times 10^{-3}$, the settling time (to 2% error of the final value for a step input) for the output response was reduced from 100 (open-loop case) to 6 ms (closed-loop case) as shown in Fig. 3(a). Therefore, the notch filter $D(s)$ enabled high-gain feedback control. Next, we show results that demonstrate feedback linearization by minimizing hysteresis and creep effects.

C. Experimental Results: High-Gain Feedback Linearization

The high-gain feedback controller described before was applied to compensate for the piezoscanner's hysteresis (and creep) behavior. By compensating for such behaviors using feedback control, we avoid the need to incorporate the creep and hysteresis behavior in the feedforward approach. We first show experimental results for hysteresis control, then we show results for creep compensation.

1) Hysteresis Compensation: Without compensation (open loop), the effect of hysteresis is significant, for exampl,e see the distortion in Fig. 4(a1) and (b1). The maximum positioning error without compensation is $e_{\max} = 18.08\%$, defined as

$$e_{\max}(\%) = \max \left| \frac{x_d - x}{\max(x_d) - \min(x_d)} \right| \times 100\% \qquad (4)$$

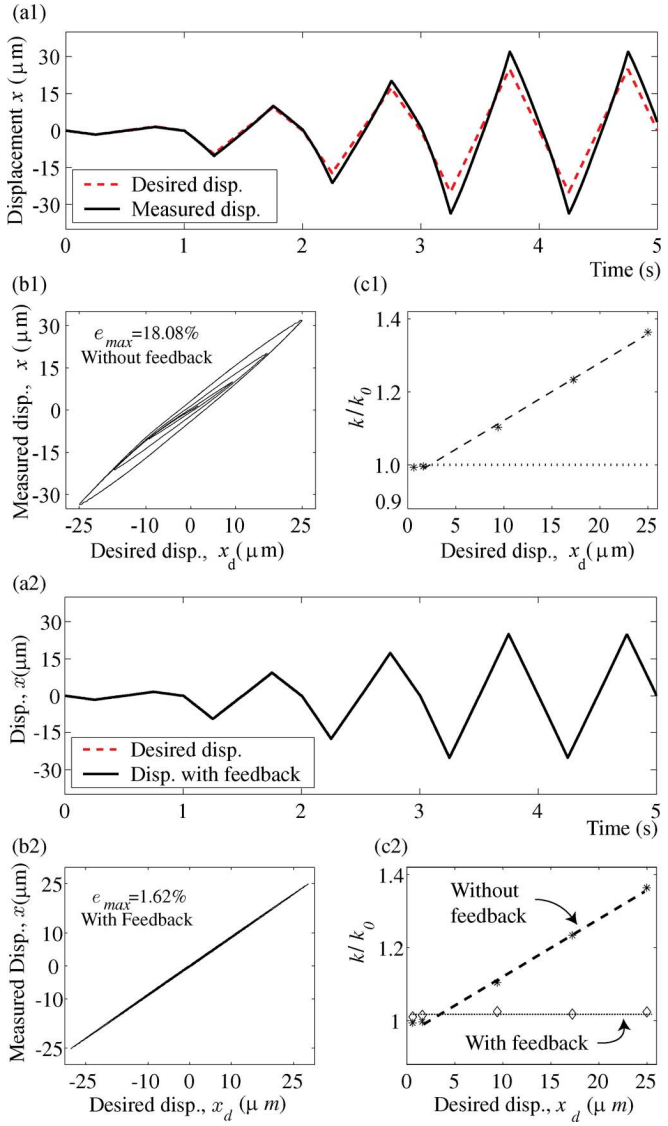

Fig. 4. Hysteresis effect and variation in the output-to-input ratio (the system gain factor) in the experimental piezoscanner system (scanning at 1 Hz). (a1)–(c1): without feedback; (a2)–(c2): with high-gain feedback. (a) Displacement versus time, (b) hysteresis curves, and (c) variation in system gain factor versus desired displacement.

where x_d and x are the desired and measured displacements in micrometers, respectively. Hysteresis can also cause the output-to-input ratio (system gain) to vary with displacement range (or equivalently, with the amplitude of the applied electric field). In terms of the model (1), the variation can be modeled as a change in the open-loop system gain factor k or the effective sensitivity of the piezoscanner changing (e.g., [7], [8], [21]). More specifically, the variation in the system's gain factor is observed by the change in slope of each individual hysteresis loop, i.e., the slope of the line connecting the turn-around points of each loop shown in Fig. 4(b1). Graphically, this variation is represented in Fig. 4(c1), a plot of the gain factor k [nondimensionalized with respect to the nominal gain factor $k_0 = 7.20 \times 10^{13}$, (1)] versus the desired displacement amplitude. In Fig. 4(c1), k increases by as much as 37% over 25-μm displacement. *The gain factor can also be affected*

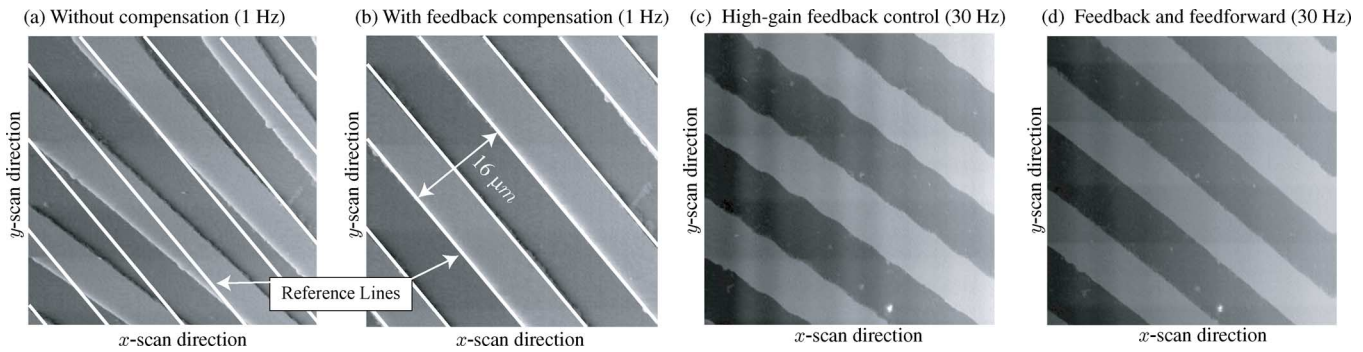

Fig. 5. AFM imaging results of calibration sample: slow speed scanning (1 Hz) (a) open-loop, without feedback compensation and (b) with high-gain feedback compensation; High-speed scanning (30 Hz) (c) high-gain feedback control and (d) high-gain with feedforward input.

by temperature [12]. We show next that high-gain feedback control minimizes the effects of hysteresis and the variation in the gain factor.

Experiments were performed to demonstrate hysteresis compensation using the proposed feedback controller and results are shown in Fig. 4(a2)–(c2). Fig. 4(a2) shows the time response of the closed-loop system for scanning at 1 Hz—slow enough that dynamics effect is negligible and fast enough that creep effect is small. The maximum scan range is 50.00 μm (i.e., $[-25.00, 25.00]$ μm). In Fig. 4(b2) (hysteresis curve), the measured displacement x is plotted versus the reference (desired) displacement $x_{\rm ref}$ for the feedback-controlled system. By applying high-gain feedback control, positioning error due to hysteresis was significantly reduced, resulting in the maximum positioning error $e_{\max} = 1.62\%$, a reduction by over 91% compared to the uncompensated case [see Fig. 4(a1) and (b1)]. Because the hysteresis distortion was drastically reduced, the variation in the closed-loop gain factor was minimized (e.g., the gain factor for the closed-loop transfer function increases by only 1.3% over 25 μm displacement [see Fig. 4(c2)]. Therefore, feedback control provides robustness to such variations. We note that additional performance improvements can be achieved with larger feedback gains, but the limitation is the gain margin of the system—30.86 dB in our case.

2) Creep Compensation: Experiments were performed to demonstrate creep compensation using the proposed high-gain feedback controller. Fig. 3(b) shows a step response measured over a period of 15 min. The measurement sampling period was 250 ms, too slow to capture the initial dynamic response of the system [5], but adequate for capturing the slow creep behavior as depicted in Fig. 3(b). Two cases were compared: 1) without high-gain feedback compensation (dashed line) and 2) with high-gain feedback compensation (solid line). The desired output displacement for both cases was 25.00 μm (dotted line). For the feedback system, to achieve the desired output range, the applied reference trajectory was the desired trajectory scaled by the measured static gain of closed-loop system, i.e., $x_{\rm ref} = 1.14 x_d$. This scaling by the static gain was used for all experiments involving only feedback control. Without feedback compensation [case 1)] the output creeps to 33.41 μm after 15 min, and the maximum positioning error as a percentage of the step range (25 μm) was $e_{\max} = 33.64\%$ (4). In contrast, the displacement measured after 15 min with high-gain feedback compensation [case 2), solid line] was 25.37 μm, resulting in the maximum positioning error $e_{\max} = 1.48\%$, a reduction by over 95% compared to the open-loop case.

3) AFM Imaging Results: The high-gain feedback method was applied to the experimental AFM to account for image distortions caused by hysteresis and creep error. A calibration sample consisting of parallel markings with a 16-μm pitch was imaged using the experimental AFM system [e.g., see Fig. 1(a) and (b)]. The imaging process was initiated by gradually moving the sample close to the probe tip until a desired (*nominal*) probe-to-sample distance (distance between the AFM-probe tip and the sample surface) was achieved. Then, the AFM-probe tip was scanned across the sample surface using the piezoscanner. During AFM imaging, the effects of the probe-to-sample distance was measured as the probe was scanned across the sample's surface. In particular, the displacement of the AFM-probe (cantilever) was measured using an optical sensor and the measurements were used to construct an image of the sample topography [see Fig. 1(a) and (b)]. An image of the surface topology was obtained by plotting the measured cantilever displacement versus the desired x and y positions of the AFM probe—this mode of operation is called the constant-height contact mode (for other AFM operating modes, see, e.g., [22]). Without feedback compensation, the image result is shown in Fig. 5(a). The features are significantly distorted due to hysteresis and creep effects; specifically, the parallel features (shown by the white reference lines) appear curved and they vary in width—the ideal features are separated by 16 μm as shown in Fig. 5(b). The distortions give an inaccurate representation of the sample surface. However, by applying high-gain feedback control, the distortions can be corrected as shown in Fig. 5(b). In Fig. 5(b), reference lines are superimposed on the image to illustrate the improvement in precision achieved by using high-gain feedback control. The results of feedback control accurately represents the actual surface topology compared to the uncompensated image with distortions shown in Fig. 5(a).

4) Bandwidth Limitations of Feedback Control: The performance of the feedback controller was evaluated for high-speed tracking of a sinusoidal reference trajectory over 50.00 μm displacement range. Fig. 6(a1)–(d1) compare the tracking for 1-, 50-, 100-, and 140-Hz scan rates and Table I(a) lists the corresponding maximum tracking error $e_{\max}$ and root-mean-square

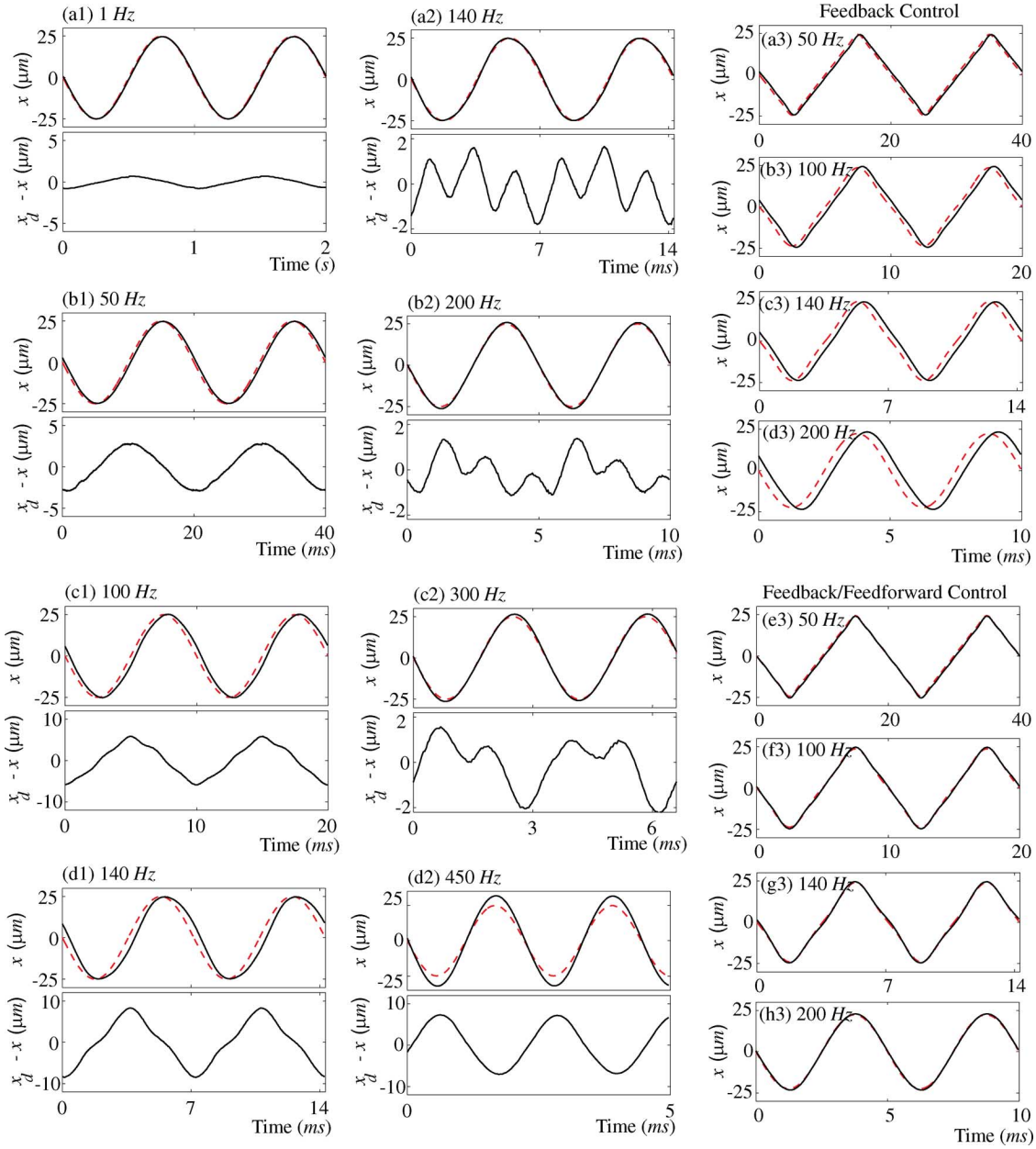

Fig. 6. Experimental results: (a1)–(d1) Tracking of sinusoidal reference trajectory using high-gain feedback control. Beyond 140 Hz, PD controller output saturates. (a2)–(d2) Tracking of sinusoidal reference trajectory using feedback and exact inverse feedforward control. (a3)–(h3) Tracking of triangular reference trajectory using feedback and optimal inversion feedforward control. Optimal weighting were chosen as $Q = 1$ and $R = 0$ for $\omega \leq 450$ Hz, and $Q = 0$ and $R = 1$ for $\omega > 450$ Hz. Solid line is the measured response and dashed line is the desired trajectory.

error e_{rms} as a percentage of the total output range (50.00 μm). For scanning at 1 Hz, the maximum error was $e_{\max} = 1.59\%$ and the root-mean-square error was $e_{\text{rms}} = 0.95\%$, defined as

$$e_{\text{rms}}(\%) = \left(\frac{\sqrt{\frac{1}{T}\int_0^T e^2(t)dt}}{\max(x_d) - \min(x_d)} \right) \times 100\% \qquad (5)$$

where T is the scanning period (e.g., scanning at 1 Hz, $T = 1$ s), and $e(t) = x_d(t) - x(t)$ is the tracking error. Overall, the experimental results show that feedback control achieves good tracking (i.e., $e_{\max} \leq 5\%$) over scan rates less than 50 Hz. However, at high speeds the effect of the dynamics becomes significant, where phase lag and vibration in the output contribute greatly to the tracking error by causing distortion in piezo positioning. Tracking error as much as 16.90% was observed for scanning at 140 Hz. At higher scan rates ($>$ 140 Hz in the experimental system), the unacceptably large error causes the feedback controller to saturate (i.e., the magnitude of the output of the op-amp circuit of the controller exceeded 10 V). Although creep and hysteresis effects are minimized, experimental results show that compensation of vibrational dynamics at high speeds using feedback control was not effective. However, we demonstrate next that adding feedforward input computed from the linear vibrational dynamics model can significantly improve the bandwidth of the closed-loop system.

TABLE I
TRACKING PERFORMANCE (a) SINUSOIDAL REFERENCE TRAJECTORY USING HIGH-GAIN FEEDBACK CONTROL. (b) SINUSOIDAL REFERENCE TRAJECTORY USING FEEDBACK-LINEARIZED EXACT INVERSE FEEDFORWARD CONTROL. (c) TRIANGULAR REFERENCE TRAJECTORY USING INTEGRATED FEEDBACK AND OPTIMAL INVERSION FEEDFORWARD CONTROL. VALUES REPORTED AS PERCENTAGE OF TOTAL OUTPUT RANGE (50.00 μm)

(a)

Scan Rate (Hz)	e_{max} (%)	e_{rms} (%)
1	1.59	0.95
50	5.79	3.93
100	11.72	7.40
140	16.90	10.38

(b)

Scan Rate (Hz)	e_{max} (%)	e_{rms} (%)
140	3.63	1.80
200	2.72	1.39
300	4.88	2.32
450	14.81	10.15

(c)

	Feedback		Integrated Feedback/Feedforward	
Scan Rate (Hz)	e_{max} (%)	e_{rms} (%)	e_{max} (%)	e_{rms} (%)
50	4.37	3.58	1.54	0.74
100	9.49	6.79	2.95	1.39
140	12.11	9.33	2.94	1.42
200	18.15	13.69	2.03	1.18

IV. HIGH-GAIN FEEDBACK AND INVERSE FEEDFORWARD CONTROL

A. Optimal Inversion

Tracking error due to vibration can be reduced by exploiting the known dynamics of the piezoscanner (e.g., see [4] and [23]). By inverting the linear dynamics model $G(s)$, a feedforward input can be found that compensates for induced structural vibrations during high-speed positioning. For a SISO system, the feedforward input is given by

$$u_{ff}(j\omega) = G^{-1}(j\omega)x_d(j\omega) \tag{6}$$

where $G^{-1}(j\omega)$ is the inverse of the system and $x_d(j\omega)$ is the desired trajectory. Equation (6) is the *exact inversion* and the Laplace transform of each term has been converted into the frequency domain by replacing s with the complex frequency $j\omega$. If the system is nonminimum phase (i.e., $G(j\omega)$ has right-half-plane zeros), the feedforward input is noncausal, but it can be computed as described in [24]. This Fourier-based inversion approach finds the feedforward inputs required to exactly track the desired trajectory x_d [25]. However, the inputs generated by (6) can be excessively large for tracking certain output trajectories, especially those containing frequency components near *lightly damped* system zeros. These large command signals can saturate the system and they can depolarize the piezoactuator. Additionally, for system models with a high degree of uncertainty over a particular frequency range, exact inversion can result in poor performance irrespective of the type of feedback controller used [17]. Therefore, we consider an optimal inversion approach to design the feedforward inputs to tradeoff tracking precision with other goals such as reduction of input energy [25]. In particular, the optimal inversion approach finds a feedforward input that minimizes the cost

$$J(u) = \int_{-\infty}^{+\infty} \big\{u^*(j\omega)R(j\omega)u(j\omega) + \big[x_d(j\omega) - x(j\omega)\big]^* Q(j\omega)[x_d(j\omega) - x(j\omega)]\big\} d\omega \tag{7}$$

where each term is expressed in the frequency domain. The superscript "*" denotes complex conjugate transpose. The cost criterion J is a design tool for trading off tracking precision with reduction of input energy by varying the relative weights between Q and R. These parameters represent frequency dependent real-valued weightings and should not be simultaneously zero at any frequency. For instance, by increasing R relative to Q, the input magnitude is reduced at the cost of tracking precision. Conversely, the tracking error is minimized by increasing Q relative to R. We point out two extreme cases for the choice of Q and R. First, if the weight on the tracking error is zero (i.e., $Q = 0$) and R nonzero, then not tracking the desired trajectory x_d would be the best approach. In the second case, if $R = 0$ and Q nonzero, then exact tracking is achieved, i.e., $x = x_d$. The solution—an input that minimizes J subject to weightings Q and R—to the optimal inversion problem is given by

$$u_{\rm opt}(j\omega) = \left[\frac{G^*(j\omega)Q(j\omega)}{R(j\omega) + G^*(j\omega)Q(j\omega)G(j\omega)}\right] x_d(j\omega) \triangleq G_{\rm opt}(j\omega)x_d(j\omega). \tag{8}$$

Applying $u_{\rm opt}(j\omega)$ to the system results in tracking of the modified desired trajectory $x_{\rm opt}$, i.e.,

$$x_{\rm opt}(j\omega) = G(j\omega)u_{\rm opt}(j\omega) = G(j\omega)G_{\rm opt}(j\omega)x_d(j\omega) \triangleq G_f(j\omega)x_d(j\omega). \tag{9}$$

In (9), $G_f(j\omega)$ is a filter that modifies the desired trajectory $x_d(j\omega)$ based on the R and Q weightings. When the optimal inversion approach is integrated with a feedback-controlled system, the modified trajectory $x_{\rm opt}$ is used as the reference trajectory to the feedback system [i.e., $x_{\rm ref} = x_{\rm opt}$ in Fig. 1(c)]. For a discussion on tradeoffs and design related issues using this technique see, for example, [17].

B. Experimental Results: Feedforward Vibration Compensation

In the first experiment, feedforward input computed offline using the exact inversion approach (6) was integrated with the high-gain feedback system for tracking a sinusoidal reference trajectory [see Fig. 1(c)]. In the second experiment, the optimal inversion method was applied to track a more general (triangular) output trajectory. Finally, AFM imaging results are shown to further illustrate the benefits of integrating feedforward input.

1) Tracking of Sinusoidal Trajectory: Results for the first experiment shown in Fig. 6(a2)–(d2) illustrate the tracking performance of a sinusoidal trajectory using feedback integrated with exact inversion feedforward control. The scan range for the experiment was 50.00 μm. Table I(b) lists the associated performance measures $e_{\rm max}$ and $e_{\rm rms}$ for 140-, 200-, 300-, and 450-Hz scan rates. The initial scan rate of 140 Hz [see Fig. 6(a2)] was chosen because it was the limit of the feedback approach [see Fig. 6(d2)]. The feedforward input was

computed using the exact inverse of $G(j\omega)$ (6) and augmented to the feedback input [i.e., the input to the piezo system is $u = u_{fb} + u_{ff}$, Fig. 1(c)]. The reference trajectory to the feedback system was the desired trajectory, i.e., $x_{\rm ref} = x_d$. The experimental results confirm that integrating dynamic-inversion feedforward inputs significantly reduces the maximum and root-mean-square of the tracking error. For example, scanning at 140 Hz using the integrated approach reduces $e_{\max}$ and $e_{\rm rms}$ by 78.52% and 82.66%, respectively, compared to using only feedback compensation for scanning at the same rate. As shown, the integrated feedback/feedforward approach achieves good tracking (i.e., $e_{\max} \leq 5\%$) beyond 300 Hz, an improvement by over six times compared to using only feedback control. Furthermore, the bandwidth of the integrated scheme was improved to 450 Hz—the feedback/feedforward controller saturates beyond this frequency.

2) Tracking of Triangular Trajectory: In this experiment, the optimal inversion approach was integrated with the feedback system to track a more general (triangular) trajectory. The results of the second experiment are shown in Fig. 6(a3)–(h3) and Table I(c). The scan range for the experiment was 50.00 μm. For the integrated feedback/feedforward scheme, the optimal input $u_{\rm opt}$ tracks the modified desired trajectory $x_{\rm opt}$, and thus the reference trajectory to the feedback system was $x_{\rm ref} = x_{\rm opt}$; recall for the feedback-only case, we chose $x_{\rm ref} = 1.14x_{\rm opt}$ (scaled by the dc gain of the closed-loop system). The weightings of the optimal inversion controller were chosen to give up tracking of all frequency components beyond 450 Hz (to avoid saturating the feedback-controlled system). In particular, the weighting values were $Q = 1$ and $R = 0$ for $\omega \leq 450$ Hz, and $Q = 0$ and $R = 1$ for $\omega > 450$ Hz. Other combinations of the weighting values can be used which considers the tradeoff between tracking performance (Q values) and input energy (R values). The results in Fig. 6(a3)–(h3) and Table I(c) demonstrate that integrated feedback and optimal inversion feedforward control substantially reduces positioning errors compared to just using feedback control for tracking a triangular trajectory—good tracking (i.e., $e_{\max} \leq 5\%$) was achieved even at 200-Hz scan rate. Furthermore, the maximum and root-mean-square of the tracking error were reduced by over 88% and 91% at this scan rate compared to using only feedback control. We point out that as the scan frequency increases, the triangular trajectory ($x_{\rm opt}$) approaches a sine wave since the optimal inversion was designed to give up tracking of frequencies beyond 450 Hz.

3) AFM Imaging Results: To illustrate the improvement in bandwidth, AFM imaging experiments were done to compare the performance of 1) high-gain feedback and 2) high-gain feedback with inverse feedforward input. A scanning frequency of 30 Hz was chosen to illustrate the method because at 30 Hz, induced structural vibration causes significant image distortion under feedback control, e.g., see the ripples in the image shown in Fig. 5(c). Since feedback control provides limited dynamic compensation at high scan rates, the vibration effect was minimized by augmenting feedforward input as shown in Fig. 5(d). Therefore, the use of feedback with feedforward input computed from the linear dynamics model avoids the need to model/invert the complex nonlinear piezo dynamics. Additionally, feedback provides robustness to parameter variation (e.g., the change in the system's gain factor k). The imaging result in Fig. 5(c) shows that the integrated approach provides a means of achieving precision positioning over a wider range of scan rates and displacements. We also note that higher performance can be achieved by using iteration to improve the feedforward input. For example, iteration-based feedforward can compensate for hysteresis [26], [27] as well as dynamic effects [28], and such inputs can be integrated with a feedback-controlled system.

V. Conclusion

We presented the design of a high-gain feedback controller to linearize the piezo dynamics such that linear feedforward input can be applied to achieve relatively high-precision high-speed positioning for an AFM system. By using a notch filter to improve the stability margin, a high-gain feedback controller was designed to account for creep and hysteresis effects without modeling the complicated nonlinear behavior. Vibration compensation was achieved by integrating with the feedback-controlled system a feedforward input computed using the linear vibrational dynamics model—the feedforward input improved the performance of the feedback controller significantly. We showed experimental results that demonstrated improved performance of an experimental AFM system over extended periods of time, long ranges, and high scan rates.

References

[1] C. Taylor, E. Stach, A. Malshe, and G. Salamo, "Nanoscale dislocation patterning by ultralow load indentation," *Appl. Phys. Lett.*, vol. 87, p. 073108, 2005.

[2] M. Bayer, G. Ortner, A. Forchel, Y. B. Lyanda-Geller, T. L. Geinecke, P. Hawrylak, S. Fafard, and Z. R. Wasilewski, "Fine structure of excitions in InAs/GaAs coupled quantum dots: A sensitive test of electronic coupling," *Phys. Rev. Lett.*, vol. 80, p. 086404, 2003.

[3] C. S. Lent, P. D. Tougaw, W. Porod, and G. H. Bernstein, "Quantum cellular automata," *Nanotechnol.*, vol. 4, pp. 49–57, 1993.

[4] D. Croft, G. Shed, and S. Devasia, "Creep, hysteresis, and vibration compensation for piezoactuators: Atomic force microscopy application," *ASME J. Dyn. Syst., Meas., Control*, vol. 123, pp. 35–43, 2001.

[5] H. Jung and D.-G. Gweon, "Creep characteristics of piezoelectric actuators," *Rev. Sci. Instrum.*, vol. 71, no. 4, pp. 1896–1900, 2000.

[6] D. C. Jiles and D. L. Atherton, "Theory of ferromagnetic hysteresis," *J. Magn. Magn. Mater.*, vol. 61, pp. 48–60, 1986.

[7] R. C. Barrett and C. F. Quate, "Optical scan-correction system applied to atomic force microscopy," *Rev. Sci. Instrum.*, vol. 62, no. 6, pp. 1393–1399, 1991.

[8] A. E. Holman, P. M. L. O. Scholte, W. C. Heerens, and F. Tuinstra, "Analysis of piezo actuators in translation construction," *Rev. Sci. Instrum.*, vol. 66, no. 5, pp. 3208–3215, 1995.

[9] Y. Okazaki, "A micro-positioning tool post using a piezoelectric actuator for diamond turning machines," *Precision Eng.*, vol. 12, no. 3, pp. 151–156, 1990.

[10] S. Salapaka, A. Sebastin, J. P. Cleveland, and M. V. Salapaka, "High bandwidth nano-positioner: A robust control approach," *Rev. Sci. Instrum.*, vol. 73, no. 9, pp. 3232–3241, 2002.

[11] M.-S. Tsai and J.-S. Chen, "Robust tracking control of a piezoactuator using a new approximate hysteresis model," *ASME J. Dyn. Syst., Meas., Control*, vol. 125, pp. 96–102, 2003.

[12] H.-J. Lee and D. A. Saravanos, "The effect of temperature dependent material properties on the response of piezoelectric composite materials," *J. Intell. Mater. Syst. Struct.*, vol. 9, pp. 503–508, 1998.

[13] P. Ge and M. Jouaneh, "Tracking control of a piezoceramic actuator," *IEEE Trans. Control Syst. Technol.*, vol. 4, no. 3, pp. 209–216, May 1996.

[14] H. Janocha and K. Kuhnen, "Real-time compensation of hysteresis and creep in piezoelectric actuators," *Sens. Actuators A*, vol. 79, pp. 83–89, 2000.

[15] S. Majima, K. Kodama, and T. Hasegawa, "Modeling of shape memory alloy actuator and tracking control system with the model," *IEEE Trans. Control Syst. Technol.*, vol. 9, no. 1, pp. 54–59, Jan. 2001.

[16] W. S. Oates and C. S. Lynch, "Piezoelectric hydraulic pump system dynamic model," *J. Intell. Mater. Syst. Struct.*, vol. 12, no. 11, pp. 737–744, 2001.

[17] S. Devasia, "Should model-based inverse inputs be used as feedforward under plant uncertainty?," *IEEE Trans. Autom. Control*, vol. 47, no. 11, pp. 1865–1871, Nov. 2002.

[18] C. J. Chen, "*In situ* testing and calibration of tube piezoelectric scanners," *Ultramicroscopy*, vol. 42–44, pp. 1653–1658, 1992.

[19] H. Y. F. Lam, *Analog and Digital Filters: Design and Realization*. Englewood Cliffs, NJ: Prentice-Hall, 1979.

[20] R. C. Dorf and R. H. Bishop, *Modern Control Systems*. Upper Saddle River, NJ: Prentice-Hall, 2001.

[21] K. R. Koops, P. M. L. O. Scholte, and W. L. de Koning, "Observation of zero creep in piezoelectric actuators," *Appl. Phys. A*, vol. 68, pp. 691–697, 1999.

[22] G. Binnig, "Force microscopy," *Ultramicroscopy*, vol. 42–44, pp. 7–15, 1992.

[23] G. Schitter and A. Stemmer, "Identification and open-loop tracking control of a piezoelectric tube scanner for high-speed scanning-probe microscopy," *IEEE Control Syst. Technol.*, vol. 12, no. 3, pp. 449–454, May 2004.

[24] Q. Zou and S. Devasia, "Preview-based stable-inversion for output tracking," *ASME J. Dyn. Syst. Meas. Control*, vol. 121, no. 4, pp. 625–630, 1999.

[25] J. S. Dewey, K. K. Leang, and S. Devasia, "Experimental and theoretical results in output-trajectory redesign for flexible structures," *ASME J. Dyn. Syst., Meas., Control*, vol. 120, pp. 456–461, 1998.

[26] K. K. Leang and S. Devasia, "Design of hysteresis-compensating iterative learning control for piezo positioners: Application to atomic force microscopes," *Mechatron.*, vol. 6, no. 3-4, pp. 141–158, 2006.

[27] G. Tchoupo and K. K. Leang, "Hysteresis compensation for high-precision positioning of a shape memory alloy actuator using integrated iterative-feedforward and feedback inputs," in *Proc. Amer. Control Conf.*, 2007, pp. 4246–4253.

[28] S. Tien, Q. Zou, and S. Devasia, "Iterative control of dynamics-coupling-caused errors in piezoscanners during high-speed AFM operation," *IEEE Trans. Control Syst. Technol.*, vol. 13, no. 6, pp. 921–931, Nov. 2005.